ELSEVIER

International Journal of Solids and Structures 41 (2004) 4219–4235

INTERNATIONAL JOURNAL OF SOLIDS and STRUCTURES

www.elsevier.com/locate/ijsolstr

Mixed-mode delamination growth in carbon–fibre composite laminates under cyclic loading

N. Blanco [a,*], E.K. Gamstedt [b], L.E. Asp [c], J. Costa [a]

[a] *Advanced Materials and Analysis for Structural Design, EPS-University of Girona, E-17071 Girona, Spain*

[b] *Department of Solid Mechanics, Royal Institute of Technology (KTH), SE-100 44 Stockholm, Sweden*

[c] *SICOMP AB, Box 104, SE-431 22 Mölndal, Sweden*

Received 16 May 2003; received in revised form 18 February 2004
Available online 2 April 2004

Abstract

Delamination growth under fatigue loads in real composite components generally develops in a non-constant propagation mode. The aim of the investigation described in this article was to develop a model capable of predicting the fatigue delamination growth in a general case, under varying mode mix conditions. The crack growth development in essentially unidirectional laminates of carbon–fibre reinforced epoxy was analysed in terms of the Paris law for different constant propagation modes: mode I (double-cantilever beam test), mode II (end-notched flexure test) and different mixed-modes I/II (mixed-mode bending test). The dependence of the Paris law parameters on mode mix is compared with the existing models in the literature. It is shown that these models do not reproduce the non-monotonic dependence on mode mix which has been observed in experimental data. Therefore, an improved phenomenological model is introduced and compared with the experimental data obtained by other researchers. To check the ability of the model to predict variable mixed-mode fatigue delamination, the mixed-mode end-loaded split test was employed and the experimental results were compared to the predictions of the model. The underlying mechanisms responsible for the dependency of the crack propagation rates on the degree of mode mix are also discussed on the basis of fractographic analysis.

Keywords: Delamination; Fatigue; Carbon–fibre composite; Mixed-mode; Paris law

1. Introduction

Most of the failures in structural elements in use are a consequence of mechanical fatigue. Therefore, fatigue is a decisive factor in designing durable mechanical elements. In laminated composite materials, the fatigue process involves different damage mechanisms that result in the degradation of the material. One of the most important damage mechanisms is the delamination between plies of the laminate. In aeronautical

* Corresponding author. Tel.: +34-972-418853; fax: +34-972-418098.
E-mail address: norbert.blanco@udg.es (N. Blanco).

0020-7683/$ - see front matter © 2004 Elsevier Ltd. All rights reserved.
doi:10.1016/j.ijsolstr.2004.02.040

applications, composite plates are sensitive to impact and delamination occurs readily in composite laminates on impact. If the composite structure is subsequently loaded in compression, delaminations are likely to grow in varying crack propagation mode and eventually cause structural failure by buckling (e.g. Nilsson et al., 2001).

Many composite components have curved shapes, tapered thickness and plies with different orientations, which will also make the delamination grow with a mode mix that depends on the extent of the crack. Thus, delaminations generally grow in mixed-mode. It is therefore important to develop methods that can characterize subcritical, mixed-mode growth in fatigue delamination. Suitable inspection intervals could then be predicted with higher accuracy.

In the present investigation, delamination growth in essentially unidirectional carbon–fibre composites was investigated in mode I, mode II and mixed-mode I/II. The mode III contribution in delamination growth was not considered because it is typically quite small for composite structures due to the constraints of adjacent plies, as shown e.g. by Jensen and Sheinman (2001) for a layered structure and by Glaessgen et al. (2002) in laminated lap-joints. In addition, the critical energy release rate values for delamination in composite laminates are higher for mode III than for the other modes (e.g. Robinson and Hodgkinson, 2000). After the experimental characterization for three different constant mode combinations in well-controlled tests by Asp et al. (2001), the propagation rates in terms of Paris-law plots were obtained. Suitable models for the dependence on the mode mix of the Paris-law parameters were explored. The existing models prescribe a monotonic dependence of the parameters with the mode mix, which is in disagreement with the observed behaviour. Therefore, an alternative non-monotonic model able to reproduce the observed behaviour was proposed.

To investigate the capabilities of this alternative non-monotonic model, experimental fatigue crack growth data obtained under non-constant mode mix (the mode mix varies as the delamination grows) was compared to the expected behaviour. The varying mode mix fatigue data was obtained using the mixed-mode end-loaded split (MMELS) test.

Finally, a fractographic study of some of the delaminated MMELS specimens is also presented in order to discuss the underlying micromechanisms that lead to the observed behaviour. Some suggestions on how to generalise the empirical growth law formulations are also given.

2. Fatigue delamination modelling

The well-known Paris law is the most commonly used method to model fatigue crack growth. In its simplest form, the Paris law can be written as:

$$\frac{\mathrm{d}a}{\mathrm{d}N} = C(\Delta G)^r \tag{1}$$

where $\mathrm{d}a/\mathrm{d}N$ is the propagation rate of the delamination, a is the delamination length, N is the number of cycles, ΔG is the total energy release rate range, and C and r are propagation parameters which must be determined experimentally. In this expression, ΔG does not take into account the individual contribution of the different modes. In the literature, other empirical expressions of the same law can be found, where the relative contributions of mode I and mode II are considered. These models are presented in Table 1 and summarised below:

Ramkumar and Whitcomb (1985) proposed a model where the propagation rate is determined by the addition of the individual propagation rates in mode I and in mode II. Gustafson and Hojo (1987) suggested a variant of the previous but depending on the energy release rate range instead of on the maximum and critical energy release rates. The model proposed by Russell and Street (1989) determines the propagation rate in mixed-mode by a linear rule of mixtures of the individual propagation rates. Dahlem and

Table 1
Models of mixed-mode delamination growth rates from the literature

Reference	Expression of the propagation law	Equation
Ramkumar and Whitcomb (1985)	$\frac{da}{dN} = C_I\left(\frac{G_I}{G_{Ic}}\right)^{r_I} + C_{II}\left(\frac{G_{II}}{G_{IIc}}\right)^{r_{II}}$	(2)
Gustafson and Hojo (1987)	$\frac{da}{dN} = C_I(\Delta G_I)^{r_I} + C_{II}(\Delta G_{II})^{r_{II}}$	(3)
Russell and Street (1989)	$\frac{da}{dN} = \left(\frac{G_I}{G_I+G_{II}}C_I + \frac{G_{II}}{G_I+G_{II}}C_{II}\right)\left(\frac{\Delta G_I}{G_{Ic}} + \frac{\Delta G_{II}}{G_{IIc}}\right)^{\left(\frac{G_I}{G_I+G_{II}}r_I + \frac{G_{II}}{G_I+G_{II}}r_{II}\right)}$	(4)
Dahlem and Springer (1994)[a]	$\frac{da}{dN} = \left[g_I\frac{E_{22}G_{Ic}}{S_{22}^2} + g_{II}\frac{E_{22}G_{IIc}}{S_{12}^2}\right](C_I^{g_I} + C_{II}^{g_{II}})\left[U\left(\frac{G_I}{G_{Ic}} + \frac{G_{II}}{G_{IIc}}\right)\right]^{(g_Ir_I + g_{II}r_{II})}$ $g_I = \frac{\frac{G_I}{G_{Ic}}}{\frac{G_I}{G_{Ic}} + \frac{G_{II}}{G_{IIc}}}; \quad g_{II} = \frac{\frac{G_{II}}{G_{IIc}}}{\frac{G_I}{G_{Ic}} + \frac{G_{II}}{G_{IIc}}}$	(5)
Kardomateas et al. (1995)	$\frac{da}{dN} = C\frac{\left(\frac{G_{Ic}G_{IIc}}{G_c}\Delta G\right)^r}{1 - \frac{G_{Ic}G_{IIc}}{G_c}G}$ $C = C_I + (C_{II} - C_I)\sin^2\psi$ $r = r_I + (r_{II} - r_I)\sin^2\psi$ $G_c = G_{IIc} + (G_{Ic} - G_{IIc})\sin^2\psi$	(6)
Kenane and Benzeggagh (1997)[b]	$\frac{da}{dN} = \exp\left[\ln(C_{II}) + (\ln(C_I) - \ln(C_{II}))\left(1 - \frac{G_{II}}{G}\right)^b\right](\Delta G)^{\left(r_I + (r_{II} - r_I)\left(\frac{G_{II}}{G}\right)^d\right)}$	(7)
Andersons et al. (2001)	$\frac{da}{dN} = C\left[\left(\frac{K_I}{K_{Ic}}\right)^2 + \left(\frac{K_{II}}{K_{IIc}}\right)^2\right]^{\frac{r}{2}}$ $r = \frac{a_1 + a_2}{\frac{a_1}{r_I} + \frac{a_2}{r_{II}}}$ $C = \left(\frac{r}{r-2}\right)\frac{a_1 + a_2}{\left(\frac{\cos\psi}{K_{Ic}}\right)^2 + \left(\frac{\sin\psi}{K_{IIc}}\right)^2}$ $a_1 = \frac{r_I - 2}{r_I}\left(\frac{\cos\psi}{K_{Ic}}\right)^2 C_I;$ $a_2 = \frac{r_{II} - 2}{r_{II}}\left(\frac{\sin\psi}{K_{IIc}}\right)^2 C_{II}$	(8)

[a] U is an effective stress ratio that can be considered to be 1 when $\Delta G \approx 0$.
[b] b and d are material parameters that must be determined experimentally.

Springer (1994) proposed a model that introduces an effective stress ratio and a dimensionless group according to the Buckingham π theorem. Kenane and Benzeggagh (1997), based on their studies on glass/epoxy laminates, suggested a modification of the Paris law where the propagation parameters depend on the relative energy release rate in mode II in a non-linear way. Based on the study of laminated materials and bimaterial interfaces, Hutchinson and Suo (1992) define the mode mix angle as $\psi = \arctan(K_{II}/K_I)$, where K_I and K_{II} are the stress intensity factors in mode I and mode II, respectively. They also assumed that the fracture toughness of the interface between the plies where the delamination grows depends on the mode mix and describe the variation of the critical energy release rate as a function of ψ. Based on these definitions, Kardomateas et al. (1995) proposed a propagation rate of the delamination where the parameters C and r also vary as functions of ψ. Andersons et al. (2001) suggested a modified Paris law as a

function of the stress intensity factors in the crack instead of the energy release rates combined with the Palmgren–Miner damage accumulation rule. The propagation parameters are also defined as a function of the critical stress intensity factors for mode I and mode II and the mode mix angle proposed by Hutchinson and Suo (1992). Table 1 summarises the expressions from the literature for the mixed-mode propagation rate and their parameters, where C_i and r_i are the propagation parameters in mode I and mode II; G_i indicates the maximum energy release rate in mode I and mode II; G_{ic} is the critical energy release rate in mode I and mode II; S_{22} is the transverse tensile strength of a unidirectional ply; S_{12} is the in-plane shear strength of the unidirectional ply and K_i and K_{ic} are the maximum and critical stress intensity factors in mode I and mode II, respectively.

In the models listed in Table 1 the mode mix dependence of the propagation parameters is only based on the propagation parameters for mode I and mode II, with the exception of the one proposed by Kenane and Benzeggagh (1997). The variation of the parameters between the extreme values is made by an empirical function of the mode mix. In all these models the dependence is monotonic. The variation of C and r in the model proposed by Kenane and Benzeggagh (1997) is based on two extra experimental factors, b and d, respectively, to account for the skewness in the mode mix dependence. These two extra parameters allow for a more complex evolution of the propagation parameters, although still in a monotonic way.

3. Experimental procedures

A series of tests was carried out to characterize the delamination growth at different mixed-modes under fatigue conditions. Some of the tests were carried out under constant mode mix in a previous investigation by Asp et al. (2001), while the rest have been carried out under varying mode mix. Basically, these tests rely on fatigue propagation from an initial delamination, or pre-crack, in beam-type specimens. All the specimens were manufactured according to the supplier's recommended procedures from unidirectional HTA/6376C carbon-epoxy prepregs produced by Hexcel. The elastic properties of the cured plies are summarised in Table 2, where '1' is in the fibre direction, '2' is in the in-plane transverse direction and '3' is in the out-of-plane direction. The average thickness of the cured plies was 0.131 mm and a 7.5 μm thick Upilex© 7.5S polyamide film, from UBE, was used as starter crack.

The fatigue delamination experiments under constant mode mix conditions were carried out in a previous investigation by Asp et al. (2001). The details of the preparation of the tests and the experimental results can be found in this publication. For mode I crack growth, a double cantilever beam (DCB) test was used. For mode II, an end-notched flexure (ENF) test was chosen. For constant 50/50 mixed-mode I/II, a mixed-mode bending (MMB) test was employed, where the energy release rate was equal for mode I and mode II, respectively.

Crack propagation tests with a slightly varying degree of mode mix were carried out with a mixed-mode end-loaded split (MMELS) test. This test is similar to the mode II end load split (ELS) test where the external load is only applied to one of the cantilever beams of the specimen. A sliding clamp end is used to avoid normal axial forces as the specimen bends. Fig. 1 represents, schematically, the test set-up for the MMELS test.

Bao et al. (1992) analysed the MMELS test using an approach based on an orthotropic rescaling technique in combination with formulae that give the best fit to finite element solutions. According to Bao et al. the results of the model for long delaminations are equivalent to the results of the models based on the

Table 2
Elastic properties of the unidirectional HTA/6376C carbon-epoxy prepreg

E_{11}	$E_{22} = E_{33}$	$\nu_{12} = \nu_{13}$	ν_{23}	$G_{12} = G_{13}$	G_{23}
120 GPa	10.5 GPa	0.30	0.51	5.25 GPa	3.48 GPa

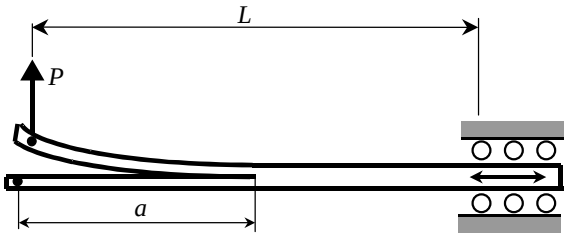

Fig. 1. Mixed-mode end-loaded split test.

first order beam theory (Hashemi et al., 1990; Kinloch et al., 1993). However, the model suggested by Bao et al. can deal with the variation of mode mix for short crack lengths. Thus, the Bao et al. model has been used for modelling the test during the present investigation. The expressions of the energy release rate according to Bao et al. for the MMELS test are as follows:

$$G = \frac{6P^2}{E_{11}b^2h_1^3}\left(1 - \left(\frac{\eta}{\eta+1}\right)^3\right)\left[a + Y(1 + F(1-\eta))\lambda^{\frac{1}{4}}h_1\right]^2 \tag{9}$$

$$G_{\mathrm{I}} = \frac{AP^2}{E_{11}b^2h_1^3}\left[a + Y_{\mathrm{I}}(1 + F_{\mathrm{I}}(1-\eta))\lambda^{\frac{1}{4}}h_1\right]^2 \tag{10}$$

where P is the load applied to the beam, b is the width of the specimen, η is the ratio between the thickness of the loaded and unloaded beams of the specimen, i.e. $\eta = h_1/h_2$, and $\lambda = E_{22}/E_{11}$. The expressions for the empirical factors Y, F, A, Y_{I} and F_{I} can be found in Bao et al. (1992). Since mode III is considered negligible, the total energy release rate is the sum of the energy release rates in mode I and mode II. The mode II energy release rate can be found from the difference of the expressions in Eqs. (9) and (10). Hence, the variation of the mode mix for this model can be calculated as a function of the delamination length.

The specimens used for the MMELS test were 20 mm wide and their effective length was $L = 150$ mm. Two different stacking sequences were considered, $[0_5/\!/(\pm5, 0_8)_{\mathrm{s}}]$ and $[0_{20}/\!/(\pm5, 0_8)_{\mathrm{s}}]$, corresponding to $\eta = 0.25$ and 1, respectively. The sign "//" refers to the plane of the artificial delamination, as shown in Fig. 2. The [±5] plies were included to reduce the fibre bridging at delamination growth. These slightly angled plies have negligible influence on the bending deformation (Davidson and Schapery, 1988). Unbridged delamination growth also plays an important role in the case of cross-over fibre bridging, since the growth conditions at the crack tip are the same as those for an unbridged crack (Sørensen and Jacobsen, 2000). Since the understanding of crack propagation of unbridged cracks is a prerequisite to address the more general case of bridged cracking, only unbridged fatigue delamination is considered at this stage.

During the testing, short initial delaminations were used to ensure a maximum variation of the mode mix. The length of the pre-cracks included in the tests, a_0, were about 2.5 and 9.5 mm for the $\eta = 0.25$ and 1 specimens, respectively. It should be mentioned that the use of such small pre-cracks increases the difficulty of obtaining reproducible fatigue delamination data with low scatter because the experiment tends to be unstable and more sensitive to local material heterogeneities. Fig. 3 shows the variation of the mode mix for the specimens tested in the MMELS test according to expressions (9) and (10). In this case, the ratio of the mode II energy release rate to the total energy release rate, G_{II}/G, is used as a measure of the mode mix instead of the mode mix angle ψ.

With the use of conventional aluminium end-blocks or piano-type hinges, the energy release rate would be difficult to estimate for short cracks due to the eccentrically applied load. To ascertain that the external load is effectively applied to the midplane of the cantilever beam, a specially designed hinge was used to

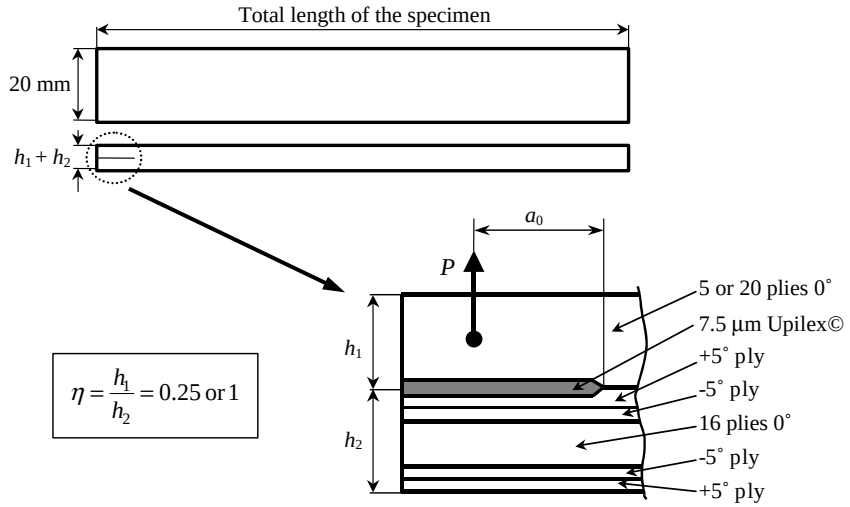

Fig. 2. Stacking sequence and initial crack for the MMELS test specimens.

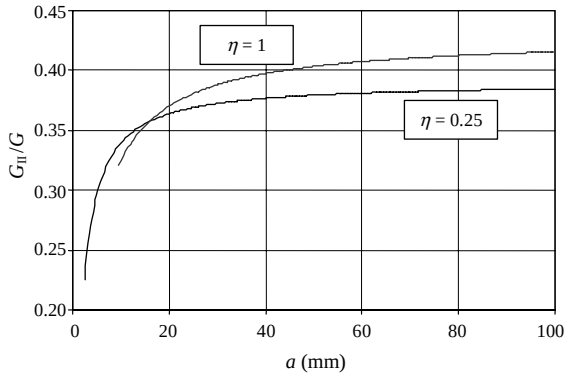

Fig. 3. Mode mix variation for the MMELS specimens according to Bao et al. (1992).

apply the load in the MMELS test. The hinge was designed to ensure a centred load in both specimen geometries. The design is a modification of the hinge design proposed by Brandt (1998). Fig. 4 shows the hinge used during the MMELS testing and how the external load is applied at the neutral plane of the upper beam of the specimen.

The specimen edges were coated with white water-base typewriter correction fluid. A transparent paper ruler with 1 mm tick intervals was glued along the edges, starting from the point where the external load was applied, to facilitate the measurement of the crack length during the test. The delamination length was measured in situ in the tensile machine along both edges of the specimen. Delamination cracks are known to form a thumb-nail shaped crack front in mode I (Schön et al., 2000). Nevertheless, because of experimental necessity, the average crack length along the edge surfaces was used in the analysis as a crack length at an effective planar front. For mixed-mode fatigue delaminations this error is deemed to be small compared with the scatter in measurements. For larger contributions of mode II, delaminations fronts have been observed to become increasingly planar (Asp et al., 2001). The specimens were tested at room tem-

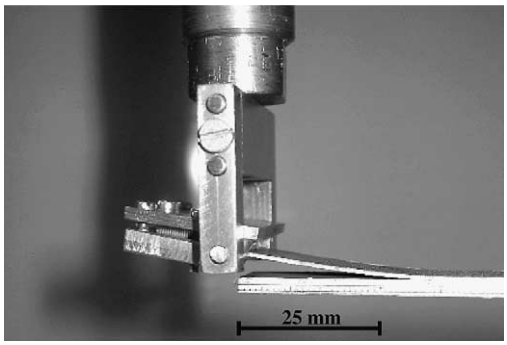

Fig. 4. Load hinge for the mixed-mode end-loaded split test.

perature in an MTS 312-21 tensile machine with the load ratio $R = P_{\min}/P_{\max} = 0.1$ and the load frequency being 2 Hz. The test was displacement-controlled and manually re-adjusted to avoid a static and unstable growth of the crack.

4. Fatigue delamination under constant mixed-mode

This section concerns the fatigue delamination tests carried out in HTA/6376C carbon-epoxy laminates by Asp et al. (2001). The tests were carried out under constant mode I (DCB), mode II (ENF) and 50/50 mixed modes I and II (MMB). The experimental propagation rates of the delamination are summarised in Fig. 5. Fitted lines for the three mode mixes are also included in the figure. For clarity, the values of the energy release rate range for each mode on the horizontal axis have been normalised by the critical energy release rate for each mode.

Despite the change in the horizontal axis, the differences between the three fitted lines are obvious. In the figure, it can be seen that the slope (the exponent r of the Paris law) for the case of the mixed-mode I/II is steeper than it is for both mode I and mode II, which are relatively similar. In addition, the intercept on the y-axis (the coefficient C of the Paris law) for the mixed-mode I/II case would not lie in between the other two. Thus, the values of the parameters C and r for the mixed-mode I/II test do not lie in between the corresponding values for mode I and mode II, as is expected for a monotonic variation. Figs. 6 and 7 show

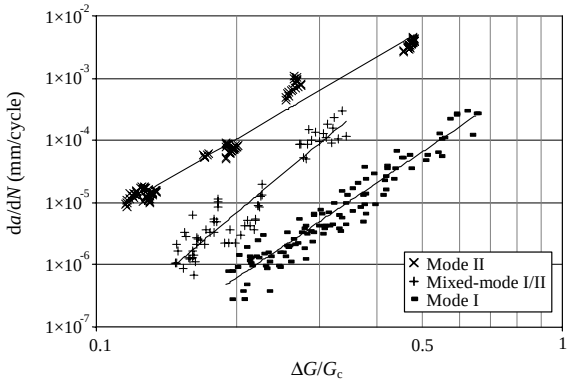

Fig. 5. Experimental fatigue propagation rates for HTA/6376C.

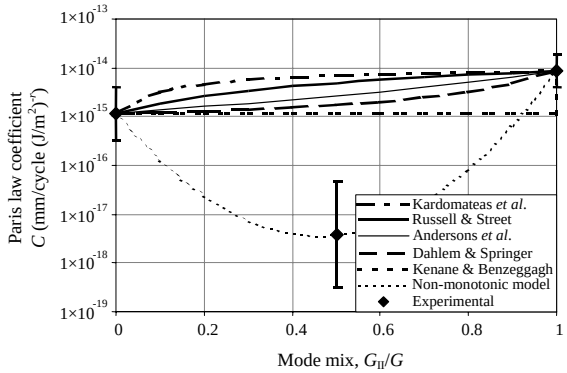

Fig. 6. Comparison of the variation of the crack propagation coefficient between the models from the literature and the experimental values of HTA/6376C.

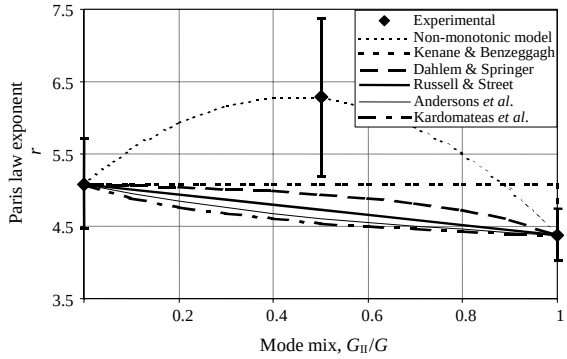

Fig. 7. Comparison of the variation of the crack propagation exponent between the models from the literature and the experimental values of HTA/6376C.

the experimental propagation parameters C and r, respectively, for the HTA/6376C carbon-epoxy laminate according to Eq. (1) as a function of the mode mix. The ratio of the mode II energy release rate to the total energy release rate, G_{II}/G, is used instead of the mode mix angle ψ. The figures also include the 95% confidence bounds for the experimental propagation parameters. The best fit for the models previously listed in Table 1 are also included. The models proposed by Ramkumar and Whitcomb (1985) and Gustafson and Hojo (1987) are, however, not included. These models predict the mixed-mode crack propagation rate as the addition of the crack propagation rates in mode I and mode II, and consequently do not lend themselves to an explicit formulation in terms of mode mix variation. Even if the model proposed by Kenane and Benzeggagh (1997) uses two extra parameters, b and d, to be adjusted to the variation of the propagation parameters, this dependency is still monotonic. The model does not account for the experimental non-monotonic variation of the growth parameters. In order to include this model in the comparison, b and d were set to zero and infinity, respectively. These values generate a Heaviside type function that best fit the experimental data, including the mixed-mode I/II data. In the figures, a non-monotonic function is also included so that a comparison can be made. This model is proposed as a consequence of the results of the present investigation, and the details are presented in the next section.

A comparison of the shape of the different curves in Figs. 6 and 7 shows that none of the models from the literature included in Table 1 are able to capture the tendency of the propagation parameters when the mixed-mode I/II is included. The values predicted by these models for this mode mix are outside the 95% confidence range. All the models are monotonic and use the mode I and mode II experimental propagation parameters to describe their development with the mode mix in a monotonic way. None of the monotonic models from the literature are therefore able to predict the non-monotonic variation of the experimental propagation parameters with sufficient accuracy for this material. Hence, the formulation of a new non-monotonic model able to capture the real variation of the propagation parameters shown in the previous figures is justified.

5. Non-monotonic model

The previously proposed models in Table 1 are formulated according to monotonic expressions of the propagation parameters with respect to the mode mix; these cannot be used, however, to describe the non-monotonic variation of the propagation parameters. For a better description of this non-monotonic variation, generalised expressions, with experimentally adjusted factors, are justified. Here, a set of parabolic equations is suggested to model the propagation parameters C and r. The expressions for both parameters are given by

$$\log C = c_1 + c_2\left(\frac{G_{\mathrm{II}}}{G}\right) + c_3\left(\frac{G_{\mathrm{II}}}{G}\right)^2 \tag{11}$$

$$r = r_1 + r_2\left(\frac{G_{\mathrm{II}}}{G}\right) + r_3\left(\frac{G_{\mathrm{II}}}{G}\right)^2 \tag{12}$$

The ratio of the mode II energy release rate to the total energy release rate is used as a measure of the mode mix. This ratio is preferred to the mode mix angle $\psi = \arctan(K_{\mathrm{II}}/K_{\mathrm{I}})$ because the dependence on ψ becomes highly skewed and does not fit the experimental data very well. In general, the polynomial coefficients c_j and r_j $(j = 1, 2, 3)$ in Eqs. (11) and (12) must be determined by a curve fitting procedure. The coefficients can be related to the propagation parameters for pure mode I and pure mode II, while extra parameters are needed to adjust the model to the mixed-mode data. Considering pure mode I, it is found that $c_1 = \log C_{\mathrm{I}}$ and $r_1 = r_{\mathrm{I}}$. Including the mode II and mixed-mode parameters, the parabolic equations become

$$\log C = \log C_{\mathrm{I}} + \log C_{\mathrm{m}}\left(\frac{G_{\mathrm{II}}}{G}\right) + \log\frac{C_{\mathrm{II}}}{C_{\mathrm{I}}C_{\mathrm{m}}}\left(\frac{G_{\mathrm{II}}}{G}\right)^2 \tag{13}$$

$$r = r_{\mathrm{I}} + r_{\mathrm{m}}\left(\frac{G_{\mathrm{II}}}{G}\right) + (r_{\mathrm{II}} - r_{\mathrm{I}} - r_{\mathrm{m}})\left(\frac{G_{\mathrm{II}}}{G}\right)^2 \tag{14}$$

where C_{m} and r_{m} are the extra mixed-mode parameters that must be determined by curve fitting. After the critical energy release rate values, G_{c}, for the HTA/6376C carbon-epoxy laminate in mode I, mode II and mixed-mode reported by Asp et al. (2001), a variation of G_{c} depending on the mode mix can be introduced. Greenhalgh et al. (1999) found a similar behaviour for different composite materials. Analogous to expressions (11) and (12), a parabolic function depending on the ratio G_{II}/G can be formulated. The expression proposed here can be seen as a modification of the mixed-mode failure criterion introduced by Yan et al. (1991), namely:

Table 3
Paris-law parameters for fatigue delamination in unidirectional HTA/6376C at different mode mixes

Test	Mode I	Mixed-mode I/II	Mode II
G_{II}/G	0	0.5	1
D (mm/cycle)	2.21×10^{-3}	1.68×10^{-1}	1.22×10^{-1}
r	5.09	6.28	4.38
G_c (J/m^2)	260	447	1002

Table 4
Propagation coefficients of Eqs. (13) and (14) for the fatigue delamination of the unidirectional HTA/6376C laminate

D_I (mm/cycle)	D_m (mm/cycle)	D_{II} (mm/cycle)	r_I	r_m	r_{II}
2.21×10^{-3}	6.09×10^{5}	1.22×10^{-1}	5.09	5.48	4.38

$$G_c = g_1 + g_2\left(\frac{G_{II}}{G}\right) + g_3\left(\frac{G_{II}}{G}\right)^2 \tag{15}$$

At this point, an expression of the Paris law is introduced, where the non-monotonic variation of the parameters is taken into account. The proposed expression is given by

$$\frac{da}{dN} = D\left(\frac{\Delta G}{G_c}\right)^r \tag{16}$$

where the parameters D, r and G_c depend on the mode mix G_{II}/G according to Eqs. (11), (12) and (15), respectively. The coefficient is now denoted by D to discriminate between the two Paris law expressions (1) and (16); D always has the unit length per load cycle, whereas the unit for C depends on the value of the exponent r. The values of these parameters for the material in this study are presented in Table 3. It is possible to fit the parabolic expressions in Eqs. (13) and (14) to these experimental results. The coefficients for these equations are summarised in Table 4.

6. Results and discussion

6.1. Validation of the non-monotonic model

The variations of the propagation parameters C and r according to the mode mix, as predicted by the non-monotonic model for the HTA/6376C carbon-epoxy laminate, are shown in Figs. 6 and 7, respectively. From the figures, it is clear that the non-monotonic model fits the experimental values of the propagation parameters better than the models included in Table 1, which is expected, since the three experimental points for each parameter are used to fit the parabolic model with three fitting parameters. Experimental work on a carbon/epoxy laminate, with more growth data for intermediate mode mixes, was presented by Tanaka and Tanaka (1995). The C and r values of the Paris law in Eq. (1) for their experimental results are plotted in Figs. 8 and 9, respectively. The figures also include the mode mix variation of the parameters according to the best fit of the monotonic models listed in Table 1. Once again, the models proposed by Ramkumar and Whitcomb (1985) and Gustafson and Hojo (1987) have been excluded for the same reasons as described before. Also as mentioned before, the model proposed by Kenane and Benzeggagh (1997) cannot account for the non-monotonic variation, even though it uses two extra parameters, b and d. To include this model in the comparison, b and d have been set to infinity and zero, respectively. The 95% confidence intervals of the experimental propagation parameters are also indicated. The curves from the

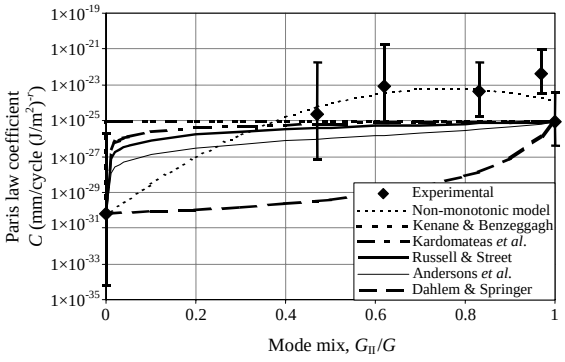

Fig. 8. Comparison of the variation of the crack propagation coefficient between the models from the literature and the experimental values of Tanaka and Tanaka (1995).

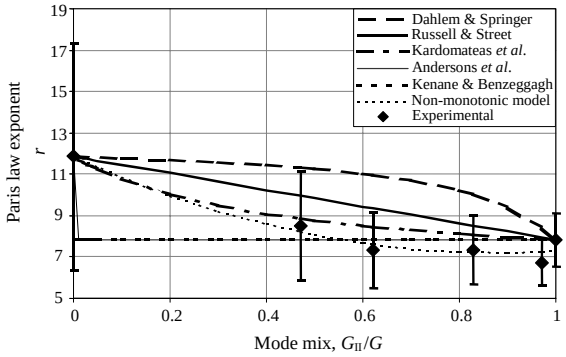

Fig. 9. Comparison of the variation of the crack propagation exponent between the models from the literature and the experimental values of Tanaka and Tanaka (1995).

non-monotonic model are also included in the figures in order to show the improved accuracy of the non-monotonic expression for the estimation of the propagation parameters.

In the previous figures, 8 and 9, it can be seen that the 95% confidence interval for the propagation parameters in mode I is significantly wide, which is primarily due to the small amount of experimental data reported for this mode by Tanaka and Tanaka (1995). It is also obvious that the models included in Table 1 correctly predict the value of the parameters for the extreme modes, mode I and mode II, while there are slight differences with the predictions of the non-monotonic model. This is due to the fact that the monotonic models only use the experimental propagation parameters in pure mode I and II to define the monotonic variation of these with the mode mix. The non-monotonic model does not provide an exact match to the experimental results in mode I and II because the coefficients of the model are determined from curve fitting of all the experimental data points. In contrast, the non-monotonic model for the intermediate mode mixes is, on the whole, more accurate. In most cases, the accuracy of the non-monotonic model is very good, and in only one case is the predicted value outside the 95% confidence band. This is not the general trend of the monotonic models considered, whose predictions are not only different from the experimental values, but are outside the 95% confidence interval in many cases.

After comparing the results from Figs. 6–9, it is clear that although there is no general trend in concavity or convexity for the different materials, the proposed non-monotonic model captures the dependence of the

propagation parameters with the mode mix in a better way. For a more quantitative comparison of the different models, the averaged sum of the squared residuals, with respect to the experimental data, can be calculated as follows:

$$\chi^2 = \sum_{i=1}^{n} \frac{(y_i - f(x_i))^2}{n} \tag{17}$$

where the y_i are the experimental values of the propagation parameters, $f(x_i)$ are the predicted values of the propagation parameters and n is the number of data. The calculated sums of the squared residuals for the different models in the figures are summarised in Table 5.

Having compared the previous figures and Table 5, it is believed that some of the monotonic models will give rather poor predictions of the mixed-mode crack propagation rate. Fig. 10 shows the comparison between the experimental crack propagation rate for the HTA/6376C carbon-epoxy laminate for a mode mix $G_{II}/G = 0.5$ and the predictions of the monotonic models. The linear regression of the experimental data is also included for comparison.

Fig. 10 clearly shows that some of the models listed in Table 1 are not able to predict accurately the crack propagation rate under a $G_{II}/G = 0.5$ mixed-mode. The figure also shows that, as expected, the predictions of the model proposed by Ramkumar and Whitcomb coincide with the predictions of the model proposed by Gustafson and Hojo. Although the model proposed by Kenane and Benzeggagh cannot be fully ad-

Table 5
Goodness-of-fit of the different models for the experimental data

Model	χ^2 HTA/6376C		χ^2 Tanaka and Tanaka (1995)	
	C [$\times 10^{-30}$] (mm/cycle (J/m^2)$^{-r}$)	r	C [$\times 10^{-46}$] (mm/cycle (J/m^2)$^{-r}$)	r
Rusell and Street	8.03	0.798	2.790	1.518
Dahlem and Springer	1.00	0.598	2.801	5.226
Kardomateas et al.	16.1	1.01	2.789	0.528
Kenane and Benzeggagh	0.44	0.475	2.789	0.357
Andersons et al.	2.40	0.927	2.793	0.357
Non-monotonic model	0	0	2.446	0.120

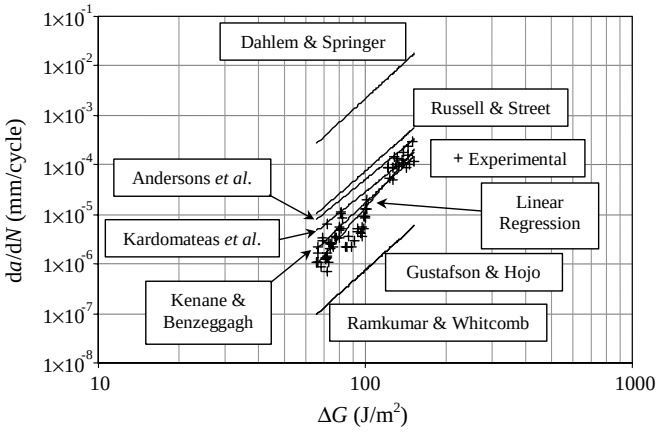

Fig. 10. Comparison of the crack propagation rate between the monotonic models from the literature and the experimental values for the HTA/6376C carbon-epoxy laminate in mixed-mode $G_{II}/G = 0.5$.

justed to the non-monotonic trend of the experimental data, it comes closest to the experimental data. However, none of these models are able to predict the actual tendency of the crack propagation rate, as indicated by the linear regression line. In other words, the models presented in Table 1 do not accurately estimate the propagation parameters C and r, which confirms that the propagation rate of the delamination depends on the mode mix in a non-monotonic way. In the figure, the prediction of the new non-monotonic model coincides with the linear regression.

6.2. Fatigue delamination growth under variable mode mix

In order to check the ability of the non-monotonic model to predict the fatigue-induced delamination growth in a non-constant mode mix situation, the mixed-mode end-loaded split (MMELS) test was employed and the experimental results compared to the predictions of the model. This test was chosen because it mimics the more realistic condition in which the mode mix varies as the delamination propagates. Due to the unstable behaviour of the MMELS test, especially for short delamination lengths, the applied load levels had to be manually readjusted to maintain a subcritical progressive delamination growth and avoid the propagation of the delamination under static conditions. However, only some of the results from the fatigue tests could be analysed. The scatter in the propagation behaviour of the fatigue-tested specimens was large. Fig. 11 shows the evolution of the delamination length versus the number of cycles for one tested specimen of each type, $\eta = 0.25$ and 1.

During the propagation of the delamination in a MMELS test, the mode mix is changing continuously; however, for sufficiently long cracks, the mode mix only varies slightly during crack propagation (as shown in Fig. 3). In Fig. 12, two Paris plots are presented based on the data in Fig. 11, in which the mode mix did not vary to any considerable degree. The experimental results are compared to the predictions of the modified Paris law, Eq. (16), including the propagation parameters D and r predicted by the non-monotonic model.

It can be seen that the simulated propagation rate, based on experimental data in constant mode mix, overestimates the propagation rate in the MMELS test, and therefore serves as a conservative prediction. The scatter between specimens was quite large, especially during the growth of short cracks. Despite these imperfections, the proposed method for predicting crack growth from constant mode mix tests is a viable route towards predicting growth during more general conditions and with better accuracy than is the case with the monotonic models (cf. Table 1). A statistical approach would, however, be preferable since the variability in data is significant. For variable mode mix during delamination growth, the crack length can be predicted by integrating Eq. (16) and taking into account the fact that the parameters D, r an G_c depend on the instantaneous mode mix according to Eqs. (11), (12) and (15) i.e.

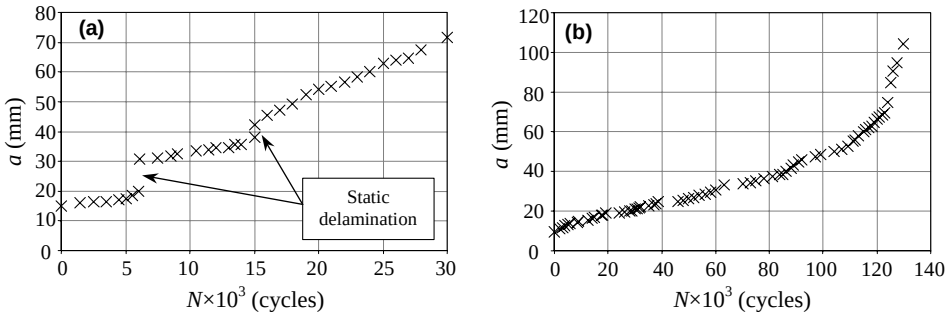

Fig. 11. Crack length versus number of cycles for the MMELS test. (a) $\eta = 0.25$ specimen and (b) $\eta = 1$ specimen.

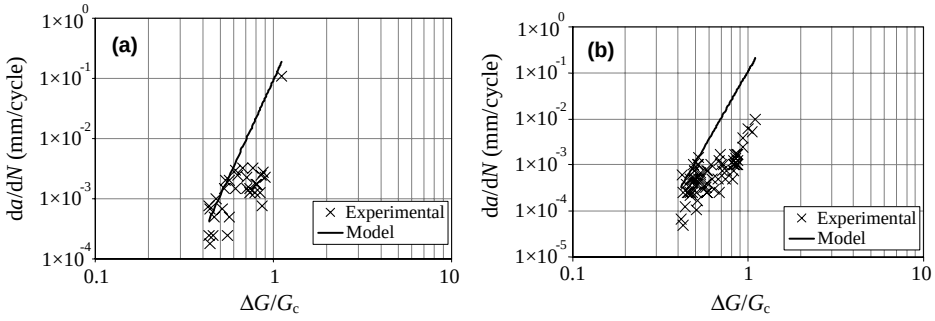

Fig. 12. Crack propagation rate versus normalised strain energy release rate for a MMELS test. (a) $\eta = 0.25$ specimen and (b) $\eta = 1$ specimen.

$$\frac{\mathrm{d}a(N)}{\mathrm{d}N} = D\left(\frac{G_{\mathrm{II}}}{G}(a)\right)\left[\frac{\Delta G(a)}{G_{\mathrm{c}}\left(\frac{G_{\mathrm{II}}}{G}(a)\right)}\right]^{r\left(\frac{G_{\mathrm{II}}}{G}(a)\right)} \tag{18}$$

where the initial delamination length is $a(0) = a_0$. The criticality of the delamination can then be assessed by comparing the maximum energy release rate $G(a)$ in Eq. (9) with the fracture toughness G_{c} in Eq. (15) at the given mode mix G_{II}/G. Suitable inspection intervals for non-destructive evaluation of the extent of delamination can also be determined, so that the composite component can be repaired or replaced before there is any risk of unstable crack growth.

6.3. Fractographic analysis

The non-monotonic behaviour depends on the micromechanisms active during delamination growth. In mode I, no friction between the arms of the specimen is observed, whereas in mode II, this is an important mechanism. In Asp et al. (2001), a fractographic analysis showed a major presence of matrix rollers for the mode II specimens. In mode II, shear microcracks are known to form in front of the crack tip, and finally coalesce to result in growth of the delamination (Singh and Greenhalgh, 1998). As the mode II component increases, a major number of micro-cracks develop into shear cusps and they become deeper in the thickness direction. Although the present lay-up has been designed to prevent fibre bridging by slightly oblique angle plies, the presence of bridging fibres cannot be ruled out. How all these micromechanisms

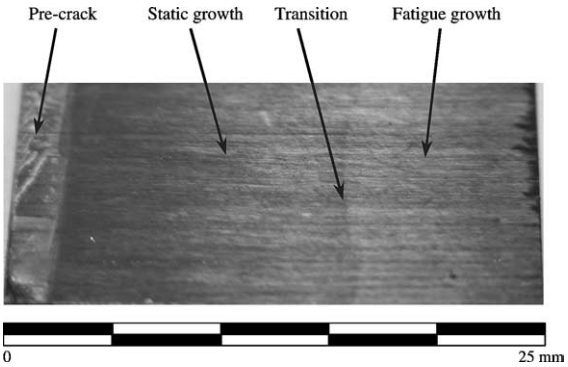

Fig. 13. MMELS delamination surface under static and fatigue growth.

combine and interact is not a well-known process, but there is no reason to believe that it should follow a linear and monotonic way for propagation rates.

After the varying mode mix fatigue tests some of the post-mortem specimens were split manually and fractographic analysis were carried out on the delaminated surfaces. By observing the delamination surfaces

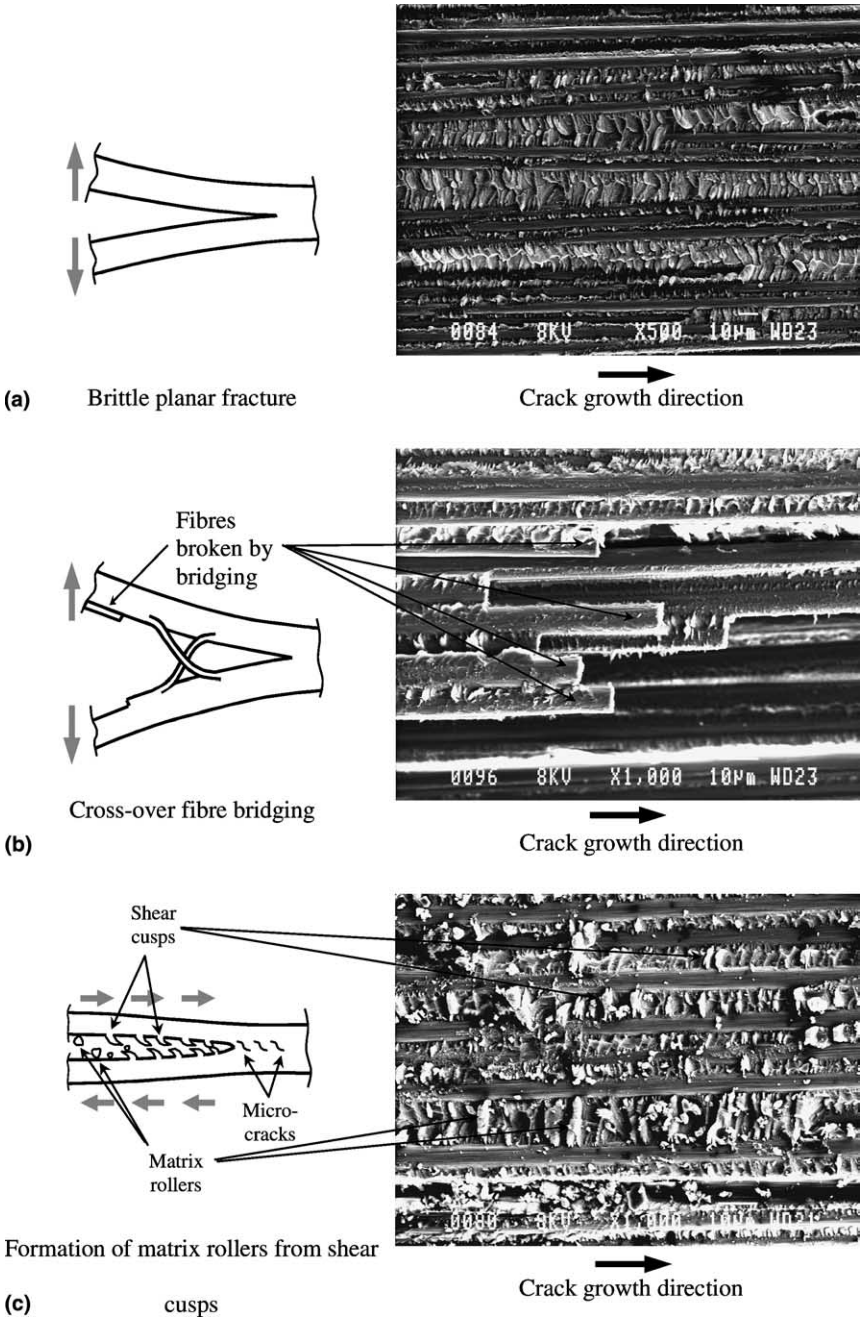

Fig. 14. Delamination micromechanisms present in the fatigue MMELS specimens.

with the naked eye, it was possible to distinguish the zones where the crack grew under static and fatigue conditions, respectively. A delaminated surface is shown in Fig. 13 where it is possible to discern three zones. The first one corresponds to the pre-crack where the thin film on the surface can still be seen. The second zone corresponds to a static delamination and the third zone corresponds to a fatigue growth. The transition between the static and fatigue regions was observed to be curved. Even if these zones were easy to distinguish by the naked eye, it was not possible to discriminate the static and the fatigue zones at high magnification when using Scanning Electron Microscope, which was also noted by Singh and Greenhalgh (1998).

Some of the previously described micromechanisms were also found during the fractographic analysis with a scanning electron microscope and are plotted schematically in Fig. 14. In some of the specimens, it was possible to find brittle planar fracture surfaces without any apparent sign of mode II delamination or fibre bridging. A scanning electron micrograph of one of these even surfaces is shown in Fig. 14(a). In some other cases the presence of fibre bridging was evident by broken fibres in the crack wake. Fig. 14(b) includes a micrograph where some fibre breaks can be seen. In other cases the existence of a certain amount of mode II fatigue delamination was clear by the presence of shear cusps and incipient matrix rollers. Some of these features can be seen in the micrograph in Fig. 14(c).

7. Conclusions

The Paris-law parameters of fatigue delamination growth in constant mode mix at different degrees of mode I and mode II have been shown to vary non-monotonically with the degree of mode mix. This is generally not taken into account in existing methodologies for growth rate predictions. A generalized model to account for this non-monotonic dependency on mode mix was presented, and applied to data from a mixed-mode end-loaded split test. The predictions show only a fair correspondence with the experimental results, although the predictions were conservative. The non-monotonic model fits the experimental growth data of intermediate mode mixes more accurately, compared with the previously presented propagation models. Fractographic analyses indicate a complex scenario of interacting fracture mechanisms, such as fibre bridging, matrix shear cracking, the formation of matrix rollers and brittle cracking, which jointly contribute to the non-monotonic behaviour of the Paris law parameters.

Acknowledgements

The authors wish to thank Mr. Hans Öberg for his help in fatigue testing with the MMELS fixture and Mr. Sören Nilsson at the Swedish Defence Research Agency (FOI) for manufacturing and supplying the test specimens. The authors would also like to show their appreciation financial support from the Spanish Government (MAT2000-0741-C02-01), the Swedish Research Council (VR) and the Swedish Defence Materiel Administration (FMV).

References

Andersons, J., Hojo, M., Ochiai, S., 2001. Model of delamination propagation in brittle-matrix composites under cyclic loading. Journal of Reinforced Plastics and Composites 20 (5), 431–450.

Asp, L.E., Sjögren, A., Greenhalgh, E., 2001. Delamination growth and thresholds in a carbon/epoxy composite under fatigue loading. Journal of Composites Technology and Research 23 (2), 55–68.

Bao, G., Ho, S., Suo, Z., Fan, B., 1992. The role of material orthotropy in fracture specimens for composites. International Journal of Solids and Structures 29 (9), 1105–1116.

Brandt, F., 1998. New load introduction concept for improved and simplified delamination beam testing. Experimental Techniques 22 (1), 17–20.

Dahlem, C., Springer, G.S., 1994. Delamination growth in composites under cyclic loads. Journal of Composite Materials 28 (8), 732–781.

Davidson, B.D., Schapery, R.A., 1988. Effect of finite width on deflection and energy release rate of an orthotropic double cantilever specimen. Journal of Composite Materials 22 (7), 640–656.

Glaessgen, E.H., Raju, I.S., Poe Jr., C.C., 2002. Analytical and experimental studies of the debonding of stitched and unstitched composite joints. Journal of Composite Materials 36 (23), 2599–2622.

Greenhalgh, E., Asp, L., Singh, S., 1999. Delamination resistance, failure criteria and fracture morphology of 0°/0°, 0°/5° and 0°/90° ply interfaces in CFRP. In: Proceedings of the 5th International Conference on Deformation and Fracture of Composites, London.

Gustafson, C.-G., Hojo, M., 1987. Delamination fatigue crack growth in unidirectional graphite/epoxy laminates. Journal of Reinforced Plastics and Composites 6 (1), 36–52.

Hashemi, S., Kinloch, A.J., Williams, J.G., 1990. The analysis of interlaminar fracture in uniaxial fibre–polymer composites. Proceedings of the Royal Society, London A 427 (1872), 173–199.

Hutchinson, J.W., Suo, Z., 1992. Mixed mode cracking in layered materials. Advances in Applied Mechanics 29, 63–191.

Jensen, H.M., Sheinman, I., 2001. Straight-sided, buckling-driven delamination of thin films at high stress levels. International Journal of Fracture 110 (4), 371–385.

Kardomateas, G.A., Pelegri, A.A., Malik, B., 1995. Growth of internal delaminations under cyclic compression in composite plates. Journal of the Mechanics and Physics of Solids 43 (6), 847–868.

Kenane, M., Benzeggagh, M.L., 1997. Mixed-mode delamination fracture toughness of unidirectional glass/epoxy composites under fatigue loading. Composites Science and Technology 57 (5), 597–605.

Kinloch, A.J., Wang, Y., Williams, J.G., Yayla, P., 1993. The mixed-mode delamination of fibre composite materials. Composites Science and Technology 47 (3), 225–237.

Nilsson, K.-F., Asp, L.E., Alpman, J.E., Nystedt, L., 2001. Delamination buckling and growth for delaminations at different depths in a slender composite panel. International Journal of Solids and Structures 38 (17), 3039–3071.

Ramkumar, R.L., Whitcomb, J.D., 1985. Characterization of mode I and mixed-mode delamination growth in T300/5208 graphite/epoxy. In: Delamination and Debonding of Materials ASTM STP 876. American Society for Testing and Materials, Philadelphia, pp. 315–335.

Robinson, P., Hodgkinson, J.M., 2000. Interlaminar fracture toughness. In: Mechanical Testing of Advanced Fibre Composites. Woodhead Publishing, Cambridge, pp. 170–210.

Russell, A.J., Street, K.N., 1989. Predicting interlaminar fatigue crack growth rates in compressively loaded laminates. In: Delamination and Debonding of Materials ASTM STP 1012. American Society for Testing and Materials, Philadelphia, pp. 162–178.

Schön, J., Nyman, T., Blom, A., Ansell, H., 2000. A numerical and experimental investigation of delamination behaviour in the DCB specimen. Composites Science and Technology 60 (2), 173–184.

Singh, S., Greenhalgh, E., 1998. Micromechanisms of interlaminar fracture in carbon fibre reinforced plastics at multidirectional ply interfaces under static and cyclic loading. Plastics, Rubber and Composites 27 (5), 220–226.

Sørensen, B.F, Jacobsen, T.K., 2000. Crack growth in composites—Applicability of R-curves and bridging laws. Plastics Rubber and Composites 29 (3), 119–133.

Tanaka, H., Tanaka, K., 1995. Mixed-mode growth of interlaminar cracks in carbon/epoxy laminates under cyclic loading. In: Proceedings of the 10th International Conference on Composite Materials 1, Whistler (Canada), pp. 181–189.

Yan, X.Q., Du, S.Y., Wang, D., 1991. An engineering method of determining the delamination fracture toughness of composite laminates. Engineering Fracture Mechanics 39 (4), 623–627.